Chinese Chemical Letters 24 (2013) 156–158

Contents lists available at SciVerse ScienceDirect

Chinese Chemical Letters

journal homepage: www.elsevier.com/locate/cclet

Original article

Synthesis of a new ratiometric emission Ca^{2+} indicator for *in vivo* bioimaging

Qiao-Ling Liu [a,b], Meng Fan [a], Wei Bian [a], Shao-Min Shuang [a], Chuan Dong [a,*]

[a] Research Center of Environmental Science and Engineering, Shanxi University, Taiyuan 030006, China
[b] Department of Chemistry, Taiyuan Normal University, Taiyuan 030031, China

ARTICLE INFO

Article history:
Received 4 November 2012
Received in revised form 29 November 2012
Accepted 5 December 2012
Available online 18 January 2013

Keywords:
Ca^{2+} indicator
Ratiometric emission
Bioimaging

ABSTRACT

A novel fluorescent calcium indicator with a 490/582 nm ratiometric emission has been designed and synthesized. The indicator exhibits a highly selective ratiometric emission response to Ca^{2+} over other metal cations and a large Stokes shift of 202 nm. Moreover, its practical cell imaging capability for intracellular Ca^{2+} in the resting- and dynamic-state has been demonstrated in human umbilical vein endothelial cells using a confocal laser scanning microscope.

1. Introduction

Calcium ion (Ca^{2+}) as an almost universal intracellular messenger plays diverse roles in intra- and intercellular signaling [1], such as gene transcription, muscle contraction and cell proliferation activities. Thus, tracking the dynamic changes of intracellular Ca^{2+} concentration would certainly assist us in recognizing many cellular processes and functions.

Fluorescent Ca^{2+} indicators as promising tools will benefit us to enhance the understanding of the physiological roles of Ca^{2+} because they can provide spatial and temporal information about the Ca^{2+} in cellular systems and *in vivo* [2]. Generally, the available Ca^{2+} indicators include intensity- and ratiometric-based indicators, and the latter is more desirable than the former in proper detection of Ca^{2+}. In the ratiometric-based Ca^{2+} indicators, only Indo-1 and Indo-5F possess ratiometric fluorescence emission behaviors toward the determination of Ca^{2+} concentration. Unfortunately, Indo-1 and Indo-5F have to subject to UV excitation and their K_d are comparatively small (0.23 and 0.47 μmol/L, respectively) so that their uses in cells and tissues are limited [3].

Herein, a novel fluorescent indicator based on ratiometric emission measurements for Ca^{2+} is synthesized. We chose 2-(4-ethoxyphenyl)-5-(4-methylphenyl)-1,3,4-oxadiazole as the fluorophore and 1,2-bis(2-aminophenoxy)ethane-*N*,*N*,*N*′*N*′-tetraacetic acid (BAPTA) group as the Ca^{2+} recognition site [4]. Due to the electron deficient property of 1,3,4-oxadiazole (OXD), when it binds to the electron rich groups of ethoxybenzene and the salt form of BAPTA, intramolecular charge transfer (ICT) from the donor to the acceptor will occur upon photon irradiation. Furthermore, owing to the permeation of OXD–BAPTA–ester, it is possible to load OXD–BAPTA–ester into living cells to monitor the intracellular Ca^{2+} concentration *in situ* by confocal microscopic imaging. Synthetic routes of OXD–BAPTA–ester and OXD–BAPTA were depicted in Scheme 1 [5].

2. Experimental

UV–vis absorption spectra were recorded on a Puxi TU-1901 UV-vis absorption spectrophotometer (China). ^{1}H NMR and ^{13}C-NMR spectra were recorded on a Bruker AVANCE III 600 NMR spectrometer (Germany). Elemental analysis was conducted on an Elementar Vario EL Cube CHNOS analyzer (Germany). Mass spectrum was acquired on a Bruker Autoflex matrix-assisted laser desorption/ionization time of flight (MALDI-TOF) mass spectrometer (Germany). Steady-state fluorescence measurements were performed on an Edinburgh FLSP 920 spectrofluorometer (UK) at 21 ± 1 °C. Synthetic routes of OXD–BAPTA–ester and OXD–BAPTA were depicted in Scheme 1, and the compound OXD–BAPTA–ester was fully characterized by ^{1}H NMR, ^{13}C NMR, mass spectrum and elemental analyses. Melting point: 62–64 °C. The ^{1}H NMR (600 MHz, $CDCl_3$): δ 8.04 (d, 2H, *J* = 4.7 Hz, Ar–H), 7.82 (d, 2H, *J* = 6.2 Hz, Ar–H), 7.56 (d, 2H, *J* = 7.5 Hz, Ar–H), 7.38 (d, 1H, *J* = 5.8 Hz, Ar–H), 7.30 (d, 1H, *J* = 5.6 Hz, Ar–H), 7.04 (d, 3H, *J* = 8.0 Hz, Ar–H), 6.91 (s, 1H, Ar–H), 6.80 (dd, 1H, *J* = 7.7 Hz, Ar–H), 6.66 (dd, 1H, *J* = 7.7 Hz and d, 1H, *J* = 6.1 Hz), 6.96 (d, 2H, *J* = 9.8 Hz, –CH=CH–), 4.60 (s, 4H, $-CH_2-CH_2-$), 4.31 (s, 8H, $-CH_2-$), 4.12 (q, 10H, *J* = 7.5 Hz, $-CH_2-$), and 1.31 (t, 15H, *J* = 5.9 Hz, CH_3-). The ^{13}C NMR (150 MHz, $CDCl_3$): δ 171, 170, 164, 161, 145, 132, 128.6, 127, 126.8, 126.7, 125.5, 121, 118, 116, 114, 110, 67,

* Corresponding author.
E-mail address: dc@sxu.edu.cn (C. Dong).

1001-8417/$ – see front matter © 2012 Chuan Dong. Published by Elsevier B.V. on behalf of Chinese Chemical Society. All rights reserved.
http://dx.doi.org/10.1016/j.cclet.2012.12.016

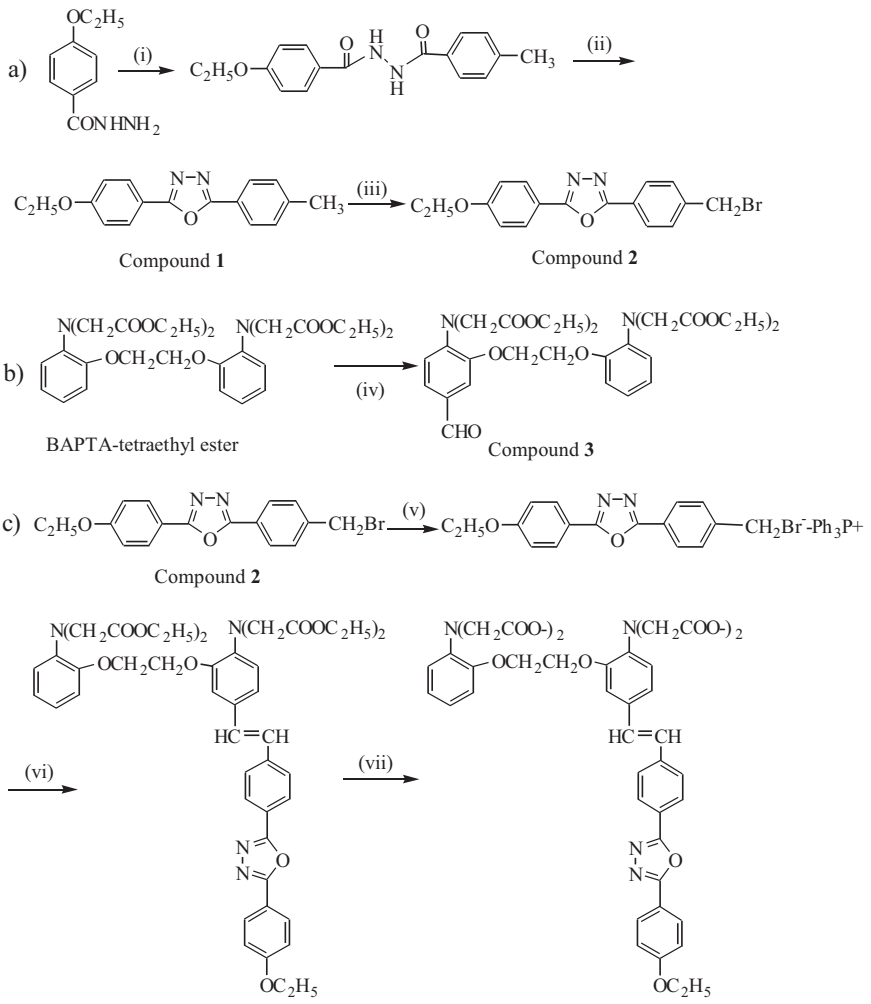

Scheme 1. Synthesis of OXD–BAPTA. (a) (i) *p*-Toluoyl chloride, Py, reflux 3 h, 90%; (ii) $POCl_3$, reflux 7 h, 60%; (iii) NBS, reflux 5 h, 90%; (b) (iv) $POCl_3$, DMF, 54%; (c) (v) Ph_3P; (vi) NaH, compound **3**, 60%; (vii) LiOH, 97%.

65.5, 61.2, 61.1, 14.7, and 14.0. MALDI-TOF MS: *m*/*z*: calcd. for $C_{48}H_{54}N_4O_{12}^+$: 878.3738; found: 901.5798 ($M+Na^+$). Elemental analysis calculated for $C_{48}H_{54}N_4O_{12}$: C 65.59, H 6.19, N 6.37, and O 21.84; found: C 65.78, H 6.20, N 6.39, and O, 21.89.

3. Results and discussion

UV–vis spectra showed that the free OXD–BAPTA in HEPES buffer solution (50 mmol/L, pH 7.2) exhibited a maximal absorbance at 380 nm. Upon addition of Ca^{2+} (0.0–11.1 μmol/L), the absorbance at 380 nm decreased gradually, and showed a blue-shift to 350 nm. When excited at 380 nm, OXD–BAPTA exhibited a maximal emission $\left(\lambda_{max}^{fl}\right)$ at 582 nm, corresponding to the free OXD–BAPTA (Fig. 1). On the addition of Ca^{2+} to OXD–BAPTA, the λ_{max}^{fl} shifted from 582 nm to 490 nm with a clear isoemissive point at 518 nm, a large blue-shift of $\Delta\lambda_{em} = 92$ nm was observed, indicating the formation of OXD–BAPTA–Ca^{2+} complex. Moreover, the ratio of emission intensity (F_{490}/F_{582}) increased linearly with the increasing Ca^{2+} concentrations; this result suggested that OXD–BAPTA can be used as a good ratiometric indicator. Due to the strong interaction between the acceptor and donor, a large Stokes shift of 202 nm was found, which implied the spectral interference from the excitation light beam and autofluorescence can be minimized. Accordingly, the fluorescence color changed from fade orange to bright green under the irradiation of an UV lamp (inset of Fig. 1).

The stoichiometric ratio for the formation of OXD–BAPTA–Ca^{2+} complex was determined by the Job's method and indicated a 1:1 ratio of OXD–BAPTA to Ca^{2+}. The dissociation constant (K_d) of OXD–BAPTA–Ca^{2+} complex was determined as 0.56 μmol/L ± 0.080 μmol/L [6]. The fluorescence quantum yields (Φ) of OXD–BAPTA

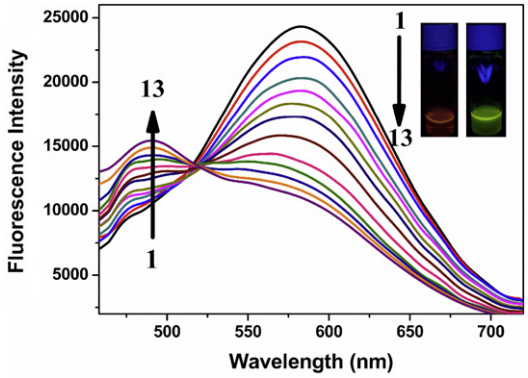

Fig. 1. Fluorescence emission spectra of 1.0 μmol/L OXD–BAPTA in 50 mmol/L HEPES (pH 7.2) containing 100 mmol/L KCl and 10 mmol/L EGTA in the presence of various concentrations of Ca^{2+} ions (1–13): 0.00, 0.026, 0.038, 0.098, 0.15, 0.227, 0.341, 0.582, 0.906, 2.04, 3.56, 5.45, and 11.1 μmol/L at excitation wavelength of 380 nm. The inset showed the fluorescence emission images of OXD–BAPTA before (left) and after (right) addition of Ca^{2+} under an UV lamp irradiation.

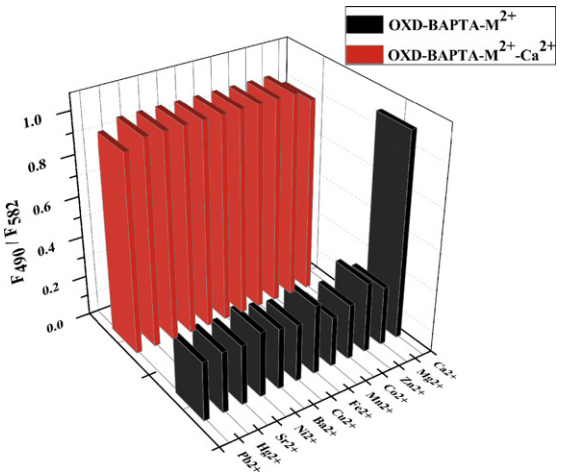

Fig. 2. Ratiometric fluorescence intensity (F_{490}/F_{582}) of 1.0 μmol/L OXD–BAPTA in the presence of 11.1 μmol/L Ca^{2+}, 150 μmol/L Mg^{2+}, Zn^{2+}, Co^{2+}, Mn^{2+}, Fe^{2+}, Cu^{2+}, Ba^{2+}, Ni^{2+}, Sr^{2+}, Hg^{2+}, Pb^{2+} (black bars) followed by adding to 11.1 μmol/L Ca^{2+} (red bars) in 50 mmol/L HEPES (pH 7.2) containing 100 mmol/L KCl. The excitation wavelength was 380 nm. (For interpretation of the references to color in this figure legend, the reader is referred to the web version of the article.)

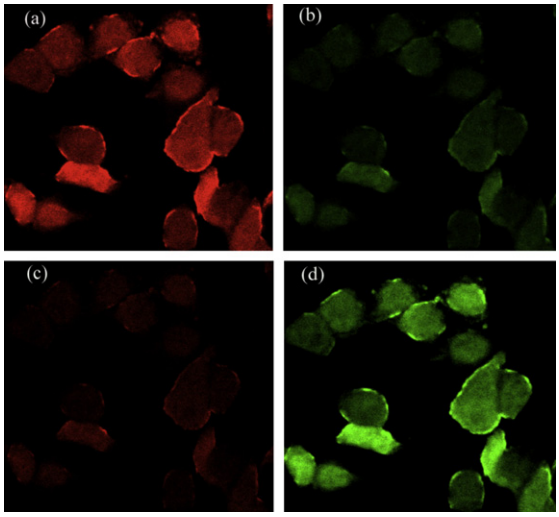

Fig. 3. Confocal fluorescence images of intracellular Ca^{2+} in living HUVEC. The excitation wavelength was 458 nm (a) and (b) OXD–BAPTA loaded HUVEC, observing emission wavelengths at 560–600 nm and 470–510 nm, respectively. (c) and (d) Penicillin G sodium salt (30 U/mL) was added to the OXD–BAPTA stained HUVEC. The images were captured after 180 s at emission wavelengths of 560–600 nm and 470–510 nm, respectively.

and OXD–BAPTA–Ca^{2+} complex were determined as 0.022 and 0.017 at excitation wavelength of 380 nm, respectively. Quinine bisulfate in 0.050 mol/L H_2SO_4 (Φ of 0.546) was used as the fluorescence standard.

The effects of various metal ions on OXD–BAPTA were also investigated under physiological conditions (Fig. 2). Ca^{2+} exhibits the largest effect on the ratiometric fluorescence intensity (490 nm/582 nm) of OXD–BAPTA, on which Mg^{2+}, Zn^{2+}, Co^{2+}, Mn^{2+}, Fe^{2+}, Cu^{2+}, Ba^{2+}, Ni^{2+}, Sr^{2+}, Hg^{2+}, Pb^{2+} have a slight effect. Thus, OXD–BAPTA can selectively detect Ca^{2+} over other metal cations.

Further studies were performed to explore the potential use of OXD–BAPTA for the detection of intracellular Ca^{2+} in living cells. Herein, OXD–BAPTA–ester was employed for its higher cell permeability. Human umbilical vein endothelial cells (HUVEC) were incubated with OXD–BAPTA–ester (5.0 μmol/L) for 40 min at 37 °C, and then the medium was removed and OXD–BAPTA stained HUVEC were washed with HEPES buffer solution three times [7]. According to the fluorescent properties of OXD–BAPTA, the optical windows at 560–600 nm and 470–510 nm were chosen for confocal imaging. Fig. 3a and b depicted images of the stained cells. These cells showed bright red and faint green fluorescence, indicating a lower free Ca^{2+} concentration in cytosol as the resting levels of $[Ca^{2+}]_i$. Then these OXD–BAPTA stained cells were given to penicillin G sodium salt (30 U/mL), the cell images were gained again after 180 s and showed in Fig. 3c and d. The images displayed that the red fluorescence dropped prominently and the green fluorescence was apparently enhanced, indicating the release of $[Ca^{2+}]_i$ from the intracellular Ca^{2+}-storing organelles after administration with penicillin G sodium salt, leading to the changes of fluorescence intensity. Thus, the increase in the ratiometric emission from the coordination between OXD–BAPTA and Ca^{2+} was clearly exhibited, rather than autofluorescence or indicator photoactivation. These results suggested that OXD–BAPTA was obviously capable of visualizing the intracellular $[Ca^{2+}]_i$ waves in living cells under a confocal laser scanning microscope.

4. Conclusion

In conclusion, we have successfully developed the ratiometric fluorescent indicator OXD–BAPTA for Ca^{2+} based on the ICT mechanism. OXD–BAPTA exhibits selective ratiometric detection for Ca^{2+} in the presence of other competing cations with a large Stokes shift of 202 nm and an obvious color change. Dual emissions and the cell-permeable nature of OXD–BAPTA–ester make it possible to study cellular Ca^{2+} in living HUVEC by confocal laser scanning microscope. These special traits indicate that OXD–BAPTA is an excellent Ca^{2+} indicator for *in vivo* bioimaging.

Acknowledgment

This work was supported by the National Natural Science Foundation of China (Nos. 21175086 and 21175087).

References

[1] (a) M.J. Berridge, M.D. Bottman, P. Lipp, Calcium-a life and death signal, Nature 395 (1998) 645–648;
(b) M. Nedergaard, A. Verkhratsky, Calcium dyshomeostasis and pathological calcium signalling in neurological diseases, Cell Calcium 47 (2010) 101–102;
(c) N. Steinckwich, V. Schenten, C. Melchior, et al., An essential role of STIM1, Orai1, and S100A8-A9 proteins for Ca^{2+} signaling and FcγR-mediated phagosomal oxidative activity, J. Immunol. 186 (2011) 2182–2191.
[2] (a) R.D. Burgoyne, Neuronal calcium sensor proteins: generating diversity in neuronal Ca^{2+} signaling, Nat. Rev. Neurosci. 8 (2007) 182–193;
(b) P. Vito, E. Lacana, L. D'Aamio, Interfering with apoptosis: Ca^{2+}-binding protein ALG-2 and Alzheimer's disease gene ALG-3, Science 271 (1996) 521–525.
[3] (a) K. Satoh, T. Matsu-Ura, M. Enomoto, et al., Highly cooperative dependence of sarco/endoplasmic reticulum calcium ATPase SERCA2a pump activity on cytosolic calcium in living cells, J. Biol. Chem. 286 (2011) 20591–20599;
(b) K.J. Buckler, Effects of exogenous hydrogen sulphide on calcium signalling, background (TASK) K channel activity and mitochondrial function in chemoreceptor cells, Pflugers Arch. 463 (2012) 743–754;
(c) T.P. Collins, D.A. Terrar, Ca^{2+}-stimulated adenylyl cyclases regulate the L-type Ca^{2+}current in guinea-pig atrial myocytes, J. Physiol. 590 (2012) 1881–1893.
[4] R.Y. Tsien, New calcium indicators and buffers with high selectivity against magnesium and protons: design, synthesis, and properties of prototype structures, Biochemistry 19 (1980) 2396–2404.
[5] X.Z. Guo, X.M. Wang, Y.K. Du, et al., Synthesis and nonlinear optical properties of new quadrupolar chromophores, Chin. Chem. Lett. 16 (2005) 597–600.
[6] G. Grynkiewicz, M. Poenie, R.Y. Tsien, A new generation of Ca^{2+} indicators with greatly improved fluorescence properties, J. Biol. Chem. 260 (1985), 3440-2450.
[7] (a) A.M.B. Reeves, E. Shigetomi, B.S. Khakh, Bulk loading of calcium indicator dyes to study astrocyte physiology: key limitations and improvements using morphological maps, J. Neurosci. 31 (2011) 9353–9358;
(b) M. Kamiya, K. Johnsson, Localizable and highly sensitive calcium indicator based on a BODIPY fluorophore, Anal. Chem. 82 (2010) 6472–6479;
(c) M. Collot, C. Loukou, A.V. Yakovlev, et al., Calcium rubies: a family of red-emitting functionalizable indicators suitable for two-photon Ca^{2+} imaging, J. Am. Chem. Soc. 134 (2012) 14923–14931.